

7.4 Magnetic properties of Praseodymium

The magnetic behaviour of Pr has already been extensively discussed in this chapter, in order to illustrate a number of the phenomena which occur in crystal-field systems. In this section, we will collect together these threads into a coherent description of the magnetic ordering which may be induced by various perturbations, and of the excitations in the paramagnetic and ordered phases.

7.4.1 Induced magnetic ordering

As discussed at the end of the preceding section, the coupling of the nuclear spins to the electronic moments in Pr gives rise to a magnetic system whose ground state is degenerate. According to the third law of thermodynamics, this degeneracy must be lifted at sufficiently low temperatures and, within the MF approximation, this is accomplished by magnetic ordering at a temperature determined by eqn (7.3.28). The enhancement factor $R_0/(1 - R_0)$ is about 12 for the hexagonal sites, so that the calculated collective-ordering temperature for the nuclear spins and the electronic moments is raised into the more readily accessible range of about 45 mK. The strong neutron-diffraction peak illustrated in Fig. 7.8 was observed at 40 mK by Bjerrum Møller *et al.* (1982), at a value of \mathbf{Q} close to the minimum in the dispersion relations of the magnetic excitons. This mode of excitation comprises magnetic fluctuations

whose zero-frequency limit is a longitudinal-wave structure along the b -axis, and the electronic moment induced by the hyperfine coupling, in the zero-temperature limit, is

$$\langle J_\eta(\mathbf{Q}) \rangle_0 \simeq IA \frac{\chi^J(0)}{1 - \chi^J(0)\mathcal{J}(\mathbf{Q})} = IA \frac{2M_\eta^2}{\Delta(1 - R_0)}, \quad (7.4.1)$$

multiplied by $g\mu_B$, corresponding to about $0.6\mu_B$. Determining the electronic moment from the neutron-diffraction intensities is complicated by the coherent nuclear scattering of neutrons at the same \mathbf{Q} , due to the induced polarization of the nuclei. The two contributions can however be separated with the help of polarized neutrons, and Kawarazaki *et al.* (1988) thereby deduced that the electronic moment on the hexagonal sites is about $0.4\mu_B$ at 30 mK, while there is also an induced moment an order of magnitude smaller on the cubic sites. The nuclear polarization on both types of site is substantial at this temperature, which is consistent with the observation by Lindelof *et al.* (1975) and Eriksen *et al.* (1983) of a dramatic increase in the nuclear heat capacity, indicating a second-order transition of the nuclear spins to an ordered structure at about 50 mK.

As may be seen in Fig. 7.8, the magnetic ordering is preceded by a strong precursor scattering, which has been observed in single crystals by a number of investigators at temperatures as high as 10 K, and was first investigated in the millikelvin range by McEwen and Stirling (1981). The figure shows that the peak actually comprises two contributions, one centred at the critical wave-vector, and a broader component at a slightly smaller wave-vector. The narrower peak, which is usually known as the *satellite*, appears around 5 K and increases rapidly in intensity as T_N is approached, at which temperature it transforms into the magnetic Bragg peak. Since the width in κ of this peak is greater than the instrumental resolution, at temperatures above T_N , it does not reflect the presence of true long-range magnetic order, but rather very intense fluctuations, with a range of several hundred Å, which presumably also vary slowly in time. The RPA theory predicts such a peak only because of the elastic scattering from the nuclear spins, as given by eqn (7.3.29). However, the peak produced by this mechanism is estimated to be visible only very close to T_N , below 200 mK, and cannot therefore explain the observations. The satellite above T_N may be interpreted as a critical phenomenon, due to the strong increase in the fluctuations, neglected in the RPA, which develop as the second-order transition is approached. When the electronic susceptibility has saturated below about 7 K, the critical fluctuations in Pr would be expected

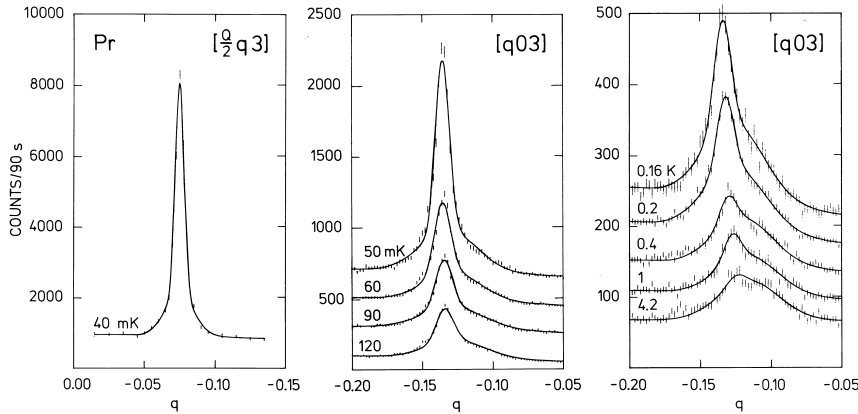


Fig. 7.8. Neutron-diffraction scans in Pr. The solid lines show the sum of two Gaussian functions fitted to the data. Only below 50 mK is the width of the narrower of these equal to the experimental resolution, indicating true long-range magnetic order.

to correspond to those of a normal degenerate system within 10% of its critical temperature. However, the satellite in Fig. 7.8 is much more intense than such fluctuations could normally give rise to. An alternative possibility, which has been analysed theoretically by Murao (1984), is that much of the intensity of the satellite above T_N is due to an ordering of the moments close to the surface of the crystal, which gives rise to a Bragg peak of non-zero width. The crystalline electric field acting on the surface ions is different from that determining the bulk properties, and the magnetic response of these ions will therefore also be different. For instance, the lowering of the symmetry near the surface splits the degeneracy of the $|\pm 1\rangle$ -states, thereby enhancing one of the basal-plane components of the susceptibility tensor.

The occurrence of the other peak in the scans shown in Fig. 7.8, known as the *central* or *quasielastic peak*, has been a long-standing mystery. It is much broader than the satellite and constitutes a ring of scattering around Γ in the basal- Γ MK-plane, with a radius which is slightly smaller than that of the contour of energy minima found in the excitation spectrum, illustrated in Fig. 7.1. The integrated quasielastic-scattering intensity from this ring is therefore rather large, and around 1 K it is found to correspond to a moment of the order of $0.1 \mu_B$ per hexagonal ion. In a polycrystalline sample, this ring of scattering cannot be distinguished from scattering from a single point in κ -space, which presumably explains why diffraction studies of polycrystalline Pr indicate that it is antiferromagnetic at 4 K (Cable *et al.* 1964).

The quasielastic peak cannot be classified as an additional critical phenomenon, because it is not centred at the critical ordering wave-vector. Furthermore, even though its intensity increases in the paramagnetic phase, as the system approaches criticality, it is still present, with a non-zero width in κ -space, below the transition and its intensity continues to increase as the temperature is further reduced (Burke *et al.* 1981; Bjerrum Møller *et al.* 1982; McEwen 1986). The dynamic effects associated with this quasielastic peak are very modest, as observed by Jensen *et al.* (1987); its width in energy is estimated to be less than 0.1 meV. Nevertheless, its integrated intensity is too large to be explained as a static phenomenon due to scattering from local *short-range* ordering of the crystal near the surface or around bulk defects, such as magnetic impurities or lattice defects. The only remaining possibility appears to be that the quasielastic peak is associated with the magnetic response of the itinerant electrons. This is consistent with one of the results of the neutron-scattering studies by Leuenberger *et al.* (1984) of the hexagonal *insulator* $\text{Cs}_3\text{Cr}_2\text{Br}_9$, in which the Cr dimers form a singlet-triplet system which has a number of analogies to Pr. Even though this system is very close to magnetic ordering, and the lowest excitation energies are only about 0.2 meV, there is no sign of either a satellite or a quasielastic peak. The spin fluctuations of band electrons are not normally expected to give rise to a quasielastic peak of the intensity observed in Pr, and its occurrence may therefore indicate the formation of resonant states near the Fermi surface in Pr, due to hybridization of the conduction electrons with the $4f$ electrons. As discussed in Section 1.3, the $4f$ electrons in Pr are very close to delocalization, and the incipient magnetic instability of the localized electrons would therefore be expected to be reflected in fluctuations in the conduction electron-gas. An indication of the sensitivity of the conduction electrons to the ordering process is provided by the resistivity measurements of Hauschultz *et al.* (1978), who found an increase of almost fifty per cent, over the temperature range in which the quasielastic peak develops, in the c -direction, where superzone effects in the ordered phase are expected to be of minor importance. Further studies of the quasielastic peak, and associated changes in the conduction electrons, particularly under high pressures with the corresponding progressive increase in $4f$ hybridization, would clearly be of interest.

Antiferromagnetism can also be induced in Pr by an internal coupling to magnetic impurities. Assuming that the susceptibility of the single impurities of concentration c is proportional to $1/T$, we find that eqns (5.6.5–6) of the virtual crystal approximation lead to an ordering temperature determined by

$$T_N = T_N(c) = \frac{c}{1 - (1 - c)R(T_N)} T_N(c = 1), \quad (7.4.2)$$

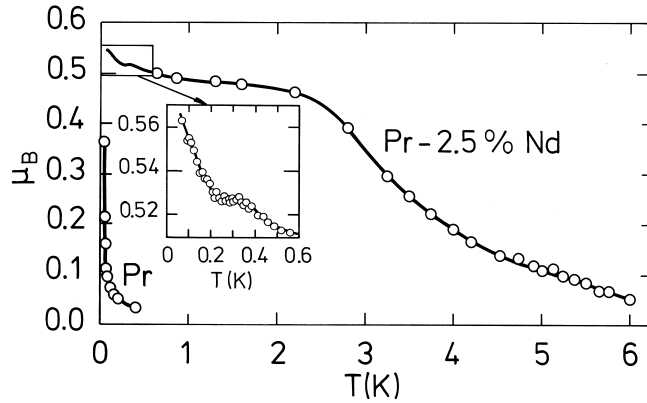


Fig. 7.9. The effective moments, deduced from the intensities of the narrower peaks in scans of the type illustrated in Fig. 7.8, in Pr and $\text{Pr}_{97.5}\text{Nd}_{2.5}$. Only below about 50 mK and 3.5 K respectively do these moments correspond to a long-range magnetically ordered state.

where $R(T)$ is the critical parameter of eqn. (7.1.6). This expression gives $T_N \simeq 12.5cT_N(c = 1)$, for $c \ll 1$. A rapid increase of T_N at small concentrations of Nd ions in Pr was indeed observed by Lebech *et al.* (1975). As illustrated in Fig. 7.9, the study of a single crystal of $\text{Pr}_{97.5}\text{Nd}_{2.5}$ by Bjerrum Møller *et al.* (1982) revealed a number of informative details. The temperature dependence of the scattered intensity follows qualitatively the behaviour observed in pure Pr. The quasielastic peak appears around 10 K, a strong satellite which is broader than the experimental resolution emerges from it around 6 K, and a diffraction peak, signifying true long-range order, develops below about 3.5 K. As in Pr, the quasielastic peak continues to grow below T_N . The rise in the magnetization below about 0.2 K is ascribed to the polarization of the nuclei and their hyperfine interaction with the $4f$ moments. Inelastic neutron-scattering experiments by Wulff *et al.* (1983) gave results consistent with a crystal-field model in which the Nd ions have a predominantly $|\pm \frac{3}{2}\rangle$ ground state, and excited $|\pm \frac{1}{2}\rangle$ and predominantly $|\pm \frac{5}{2}\rangle$ states at about 0.3 meV and 1.2 meV respectively.

The application of an external uniaxial pressure along the a -axis in the basal plane lifts the degeneracy of the $|\pm 1\rangle$ first excited-state and may therefore induce magnetic ordering, as predicted by Jensen (1976a) and observed by McEwen *et al.* (1978). The magnetoelastic phenomena described in Section 7.3.1, particularly the magnitude of the field-induced interaction between the magnetic excitations and the transverse phonons, may be used for estimating the coupling parameter $B_{\gamma 2}$

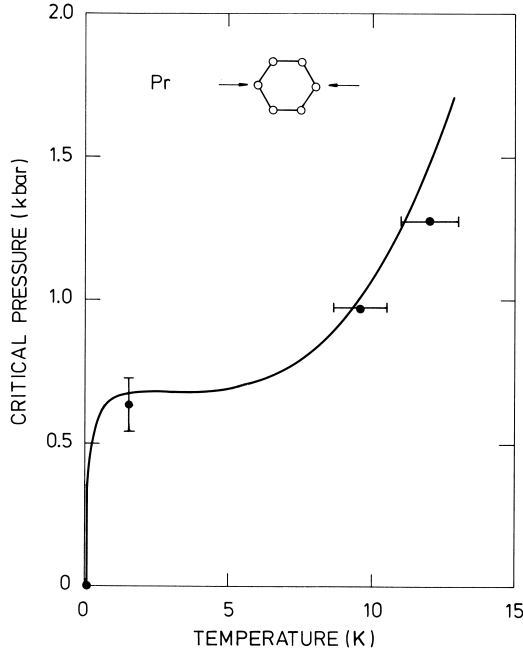


Fig. 7.10. MF calculation of the ordering temperature T_N in Pr, as a function of the uniaxial pressure in the a -direction, compared with the neutron-diffraction measurements of McEwen *et al.* (1983).

for the hexagonal ions. Neglecting the magnetoelastic coupling to the cubic ions, we obtain from eqn (7.3.2) the following γ -strain contribution to the magnetic Hamiltonian:

$$\mathcal{H}_\gamma(\text{sta}) = - \sum_{i \in \text{hex.ions}} B_{\gamma 2} O_2^2(\mathbf{J}_i) \left[\frac{1}{2} B_{\gamma 2} \langle O_2^2(\mathbf{J}_i) \rangle + t_{11} \right] / c_\gamma + \mathcal{H}_\gamma^0, \quad (7.4.3)$$

in the presence of a uniaxial stress along the ξ -axis. N in (7.3.2) is the total number of ions, or twice the number of hexagonal sites. At zero temperature and zero magnetic field, the only effect of $\mathcal{H}_\gamma(\text{sta})$, within the effective ($J = 1$)-model, is that the crystal-field splitting which determines the excitation spectrum becomes different for the two polarizations, and for instance Δ_η , giving the J_η -mode energies, is found to be

$$\Delta_\eta = \Delta_\eta(t_{11}) = \Delta - B_{\gamma 2} M_{22} t_{11} / c_\gamma,$$

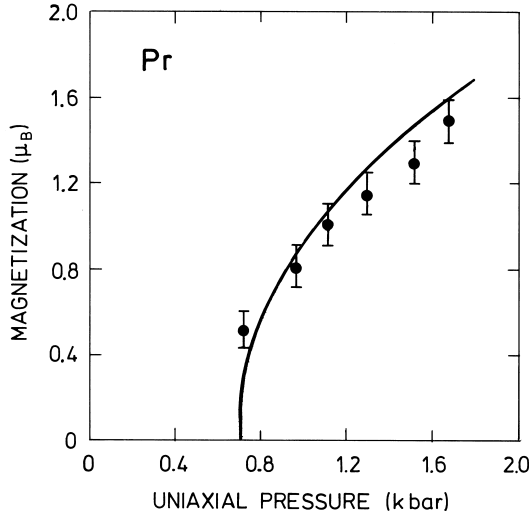


Fig. 7.11. Experimental measurements of the first harmonic of the magnetization on the hexagonal sites in Pr, deduced from the intensities of neutron-diffraction peaks at 1.5 K, compared with a MF calculation for the $J = 4$ ion.

where the matrix element

$$M_{22} \equiv \langle 1_a | O_2^2 | 1_a \rangle = - \langle 1_a | J_\eta^2 | 1_a \rangle = -10,$$

in Pr. Δ_ξ differs from Δ by the same amount, but with the opposite sign. At the incipient ordering wave-vector \mathbf{Q} along the η -axis, the excitations are purely transverse or longitudinal, J_ξ or J_η modes. The critical ratio R_0 , defined by eqn (7.1.6), for the optical longitudinal mode at \mathbf{Q} is then determined by

$$R_0(t_{11}) = R_0(0) \Delta / \Delta_\eta(t_{11}).$$

Hence the application of the stress alters the critical ratio, and it attains the threshold value 1 when

$$T_{11}^c = \frac{\{1 - R_0(0)\} \Delta}{M_{22} B_{\gamma 2}} c_\gamma N/V, \quad (7.4.4)$$

where $c_\gamma N/V = 4c_{66}$. With the following values of the parameters; $R_0(0) = 0.92$, $\Delta = 3.52$ meV, $B_{\gamma 2} \simeq 12$ meV, and $c_{66} = 1.6 \cdot 10^{10}$ N/m², the effective ($J = 1$)-model predicts that the critical stress necessary for inducing magnetic ordering in Pr at zero temperature is $T_{11}^c = -1.5$ kbar. However, the $|3_s\rangle$ -state lies just above the magnetic excitons

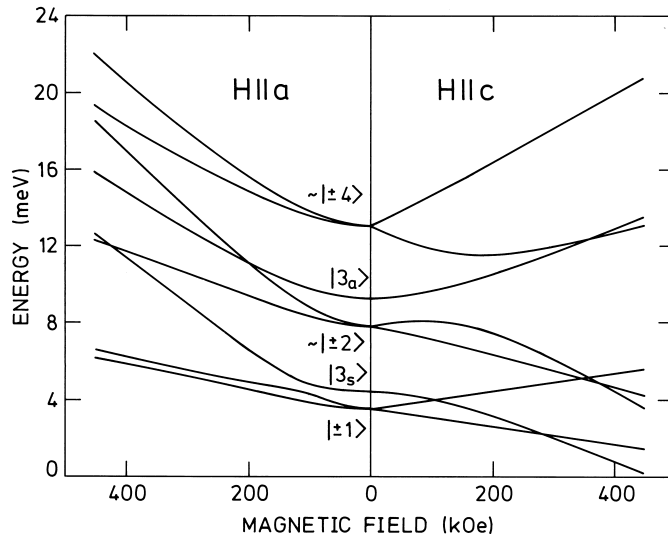


Fig. 7.12. The crystal-field levels of an isolated hexagonal ion in Pr, as a function of an applied magnetic field in the a - and c -directions. The zero-field wavefunctions are specified more precisely in Fig. 1.16.

and, as $\langle 1_a | O_2^2 | 3_s \rangle$ is non-zero, it has a significant effect on $\Delta_\eta(t_{11})$. A calculation which includes all the crystal-field levels of Pr predicts the critical uniaxial pressure $-T_{11}^c$ along the ξ -axis to be 0.7 kbar. As may be seen in Fig. 7.10, such a calculation is in good agreement with the experimental observations of McEwen *et al.* (1983), at temperatures sufficiently high that the hyperfine coupling is of no importance, and also accounts very well for the critical pressure at higher temperatures, where the thermal population of the magnetic excitons becomes significant. The dependence of the ordered moment at 1.5 K on the uniaxial pressure is also very well reproduced by this theory, as illustrated in Fig. 7.11. The stable configurations of the moments at zero pressure are expected to be analogous to those found in Nd and discussed in Sections 2.1.6 and 2.3.1, i.e. a single- \mathbf{Q} structure at small values of the magnetization and a double- \mathbf{Q} configuration when the first harmonic of the moments is larger than about $0.2\text{--}0.3\mu_B$. This behaviour has not been established experimentally, but a suggestive rotation of the ordering wave-vector away from the symmetry axis, as expected in the double- \mathbf{Q} structure, has been detected (McEwen *et al.* 1983). Uniaxial pressure stabilizes a longitudinal wave with \mathbf{Q} along the b -axis perpendicular to the strain, and a modest pressure of about 0.1 kbar is estimated to be sufficient to quench the double- \mathbf{Q} structure. Accordingly, the theoretical curve in

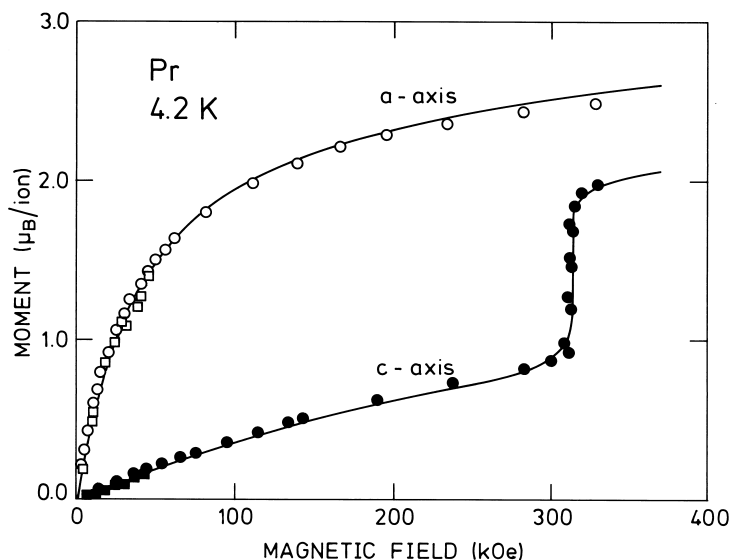


Fig. 7.13. MF calculation of the magnetization of Pr at 4.2 K as a function of a magnetic field applied in the a - and c -directions. The circles are the experimental measurements of McEwen *et al.* (1973), while the squares are deduced from the neutron-diffraction results of Lebeck and Rainford (1971).

Fig. 7.11 is calculated with the assumption of a single- \mathbf{Q} ordering of the moments.

The final perturbation which may induce a magnetic state in Pr is an external magnetic field. The modification of the crystal-field levels of an isolated hexagonal ion by a magnetic field is illustrated in Fig. 7.12. If the field is in the basal plane, the excited states are increased in energy, relative to the ground state, but they mix strongly into it, giving rise to the large moment shown in Fig. 7.13. If the magnetic field is along the c -axis, on the other hand, the matrix elements between the ground and excited states on the hexagonal sites are zero, but the $|+1\rangle$ and $|3_S\rangle \rightarrow |+3\rangle$ states both decrease in energy, linearly and quadratically respectively. At about 320 kOe, the latter crosses the ground state and the moment increases abruptly, as observed by McEwen *et al.* (1973). As illustrated in Fig. 7.13, the model of Houmann *et al.* (1979), supplemented with a magnetoelastic coupling $B_{\alpha 2} = 7.0$ meV for the hexagonal ions, accounts well for these results. The jump in the magnetization rapidly becomes smeared out when the temperature is raised, due to the thermal population of the excited states, as observed experimentally at 14 K (McEwen 1978).

7.4.2 The magnetic excitations

The magnetic-excitation spectrum in Pr has been investigated experimentally in great detail as a function of various external constraints, such as the temperature, a magnetic field applied in the basal plane, and uniaxial pressure. Most of the knowledge about the (low-temperature) coupling parameters in the model Hamiltonian for Pr, which we have already utilized several times in the preceding sections, has been derived from these experiments. The first inelastic neutron-scattering experiments on Pr (Rainford and Houmann 1971; Houmann *et al.* 1975b) showed that the excitations behave as expected in a singlet ground-state system, and that the two-ion coupling is just below the threshold value for inducing magnetic ordering. A MF analysis of the temperature dependence of the excitations, shown by the dashed lines in Fig. 7.3, indicated that the crystal-field splitting Δ between the $|0\rangle$ ground-state and the first excited $|\pm 1\rangle$ -doublet state of the hexagonal ions is about 3.2 meV. An important discovery (Houmann *et al.* 1975b) was the observation, illustrated in Fig. 7.1, of a strong splitting of the doublet excitations, whenever such a splitting is allowed by symmetry, i.e. when \mathbf{q} is not along the c -axis. This effect demonstrates that the anisotropic contribution to the two-ion Hamiltonian of Pr,

$$\begin{aligned} \mathcal{H}_{JJ} = & -\frac{1}{2} \sum_{ij} \mathcal{J}(ij) \mathbf{J}_i \cdot \mathbf{J}_j \\ & + \frac{1}{2} \sum_{ij} \mathcal{K}(ij) [(J_{i\xi} J_{j\xi} - J_{i\eta} J_{j\eta}) \cos 2\phi_{ij} + (J_{i\xi} J_{j\eta} + J_{i\eta} J_{j\xi}) \sin 2\phi_{ij}], \end{aligned} \quad (7.4.5)$$

is important. Here ϕ_{ij} is the angle between the ξ -axis and the projection of $\mathbf{R}_i - \mathbf{R}_j$ on the basal plane. Real-space coupling parameters $\mathcal{J}(ij)$ and $\mathcal{K}(ij)$ derived from the excitation energies shown in Fig. 7.1, using the MF-RPA expression for the energies with $\Delta = 3.52$ meV, are shown in Fig. 1.18. This somewhat larger value of Δ was obtained from a study of the field dependence of the excitations (Houmann *et al.* 1979), but it is still consistent with their temperature dependence, as shown by the results of the self-consistent RPA, the solid lines in Fig. 7.3. Besides leading to the more accurate value of Δ , the field experiments revealed the presence of a rather strong magnetoelastic γ -strain coupling in Pr, which creates energy gaps proportional to the field at the crossing points of the magnetic-exciton and transverse-phonon branches in the basal-plane directions, as illustrated in Fig. 7.14.

The model Hamiltonian, with the two-ion and magnetoelastic terms given respectively by (7.4.5) and (7.4.3), together with the usual single-ion crystal-field Hamiltonian for a hexagonal system, describes very well the excitation-energy changes observed by Houmann *et al.* (1979) when

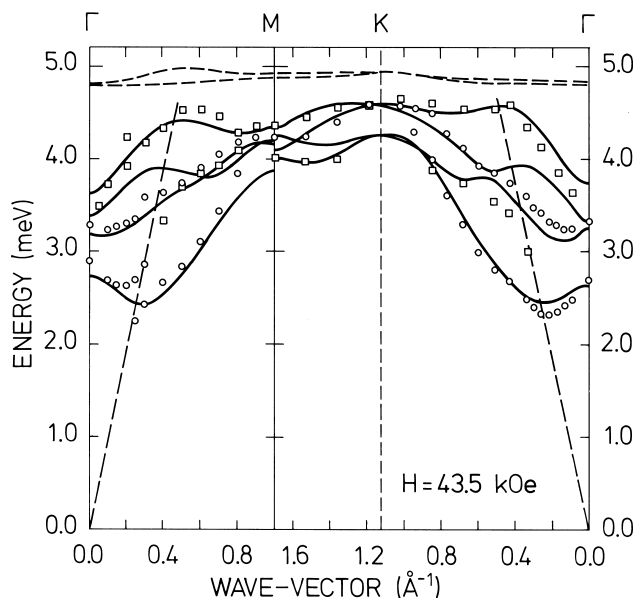


Fig. 7.14. Dispersion relations for the excitations propagating on the hexagonal sites of Pr at 6 K, in an applied field of 43.5 kOe. The field is in the basal plane and perpendicular to the wave-vector, so that there is a discontinuity at M, corresponding to a rotation of the field through 90° . Compared with Fig. 7.1, the energy of the magnetic excitations has increased, and the field has induced couplings between the magnetic excitations and the transverse-acoustic phonons polarized in the basal plane, indicated by dashed lines. These phonons are coupled to the acoustic and optical longitudinal magnetic modes in the ΓM -direction, and to the (predominantly) acoustic longitudinal and optical transverse modes (the two branches of intermediate energy) in the ΓK -direction (Jensen 1976a). The full lines show the results of an RPA calculation of the magnetic excitations, neglecting the coupling to the phonons. The predicted low-intensity higher-lying modes, corresponding to transitions to the predominantly $|3_S\rangle$ crystal-field state, were not observed directly in the experiments, but their influence may be seen in the lowest branch along ΓK , since it is their mixing with this mode which holds the energies below those along ΓM .

a field is applied in the basal plane at low temperature. The dispersion relation was measured at three values of the field (14.5, 29.0, and 43.5 kOe), and the results obtained at the highest field are shown in Fig. 7.14.

The most important effect of the field is the admixture of $|1_{S,a}\rangle$ into the ground state. This causes Δ_ξ and Δ_η to increase, and the matrix elements M_ξ and M_η to decrease. The energies of the excita-

tions are thereby increased, while the dispersion becomes smaller. If the field is applied along the ξ -axis, the ξ -mode parameters are changed approximately twice as much, relative to their zero-field values, as the η -mode parameters. At $H = 43.5$ kOe, the total molecular field, which determines the energies in Fig. 7.12, is 100 kOe, and $\Delta_\xi = 4.29$ meV, whereas $\Delta_\eta = 3.86$ meV. This means that the field produces the largest effects on the excitations polarized (predominantly) parallel to it, which in Fig. 7.14 are the transverse modes, both when \mathbf{q} is along ΓM and along ΓKM . The γ -strain coupling opposes the splitting of the transverse and longitudinal modes, but only quadratically in the field. The hexagonal anisotropy does not affect the effective ($J = 1$)-excitations in zero field, but B_6^6 causes a splitting between the $|3_s\rangle$ and $|3_a\rangle$ -states of nearly 5 meV. As B_6^6 is negative, the lower of the two states is $|3_s\rangle$ which, according to Fig. 1.16 or 7.12, should lie only 0.9 meV above the $|1_{s,a}\rangle$ -states. The magnetic field induces a coupling between this neighbouring level and the doublet excitations, so that it acquires a significant scattering cross-section at the energies indicated by the dashed lines in Fig. 7.14. Although the extra peak was not sufficiently distinct to be detected directly in the neutron-scattering experiments, the presence of this level is clearly manifested in the behaviour of the doublet excitations. The absolute minimum in the excitation spectrum at zero field is found along ΓM , whereas at $H = 43.5$ kOe the energy minimum in the ΓK -direction has become the lowest. The $|3_s\rangle$ -excitations are coupled to the doublet excitations polarized along the ξ -axis, both when the field is along the ξ - and the η -axis. This means that the energy increase of the longitudinal (optical) mode in the ΓK -direction is diminished, due to the repulsive effect of the field-induced coupling to the $|3_s\rangle$ -excitations. When the field is along the ξ -direction, the longitudinal modes in the ΓM -direction are coupled to the $|3_a\rangle$ -excitations, which lie at much higher energies and only perturb the lower modes very weakly. The basal-plane anisotropy is also clearly reflected in the field dependence of the elastic constant c_{66} , shown in Fig. 7.5.

The effects of the field on the hexagonal doublet-excitations are very strong. In comparison with the zero-field result of Fig. 7.1, the minimum-energy modes have more than doubled their energies, while the overall width of the excitation bands has been reduced by nearly a factor of two. Because of these large changes, the measurement of the field dependence of the excitation spectrum allowed a rather precise determination of Δ and the relative position of the $|3_s\rangle$ crystal-field level. With the assumption that $B_6^6 = -(77/8)B_6^0$, these results then led to the crystal-field level-scheme for the hexagonal ions shown in Figs. 1.16 and 7.12, leaving only the position of the highest-lying level somewhat arbitrary. The field experiment also determined the value of

the magnetoelastic parameter $(B_{\gamma_2})^2/c_\gamma$. This agrees with the value of B_{γ_2} for the hexagonal ions which accounts for the coupling between the magnetic excitations and the phonons, and for the field dependences of c_{66} (Fig. 7.5) and of the γ -strains (Hendy *et al.* 1979). It furthermore allowed the accurate prediction of the strain-induced antiferromagnetic transition in Pr, shown in Fig. 7.10.

The low-temperature magnetic properties of Pr are dominated by the hexagonal ions. One consequence of this is that it is more difficult to construct a reliable model for the cubic ions, based on experimentally derivable parameters. Although the model proposed by Houmann *et al.* (1979) accounts accurately for the bulk of the low-temperature experimental results, it is not uniquely specified and some deficiencies appear in comparison with experiments at elevated temperatures. The model is based on the following crystal-field Hamiltonian for the cubic ions:

$$\mathcal{H}_J = \sum_{i \in \text{cub. ions}} \left[B_4^0(c) \{ O_4^0(\mathbf{J}_i) - 20\sqrt{2} O_4^{-3}(\mathbf{J}_i) \} \right. \\ \left. + B_6^0(c) \{ O_6^0(\mathbf{J}_i) + \frac{35}{4}\sqrt{2} O_6^{-3}(\mathbf{J}_i) - \frac{77}{8} O_6^6(\mathbf{J}_i) \} \right], \quad (7.4.6)$$

which neglects the departure of the local symmetry of these sites from cubic. We shall not present an extensive discussion of the model here (more details may be found in Houmann *et al.* (1979) and Jensen (1979b, 1982)), but it is clear that this MF model, which is the simplest description of Pr consistent with its magnetic behaviour in the low-temperature limit, must be extended in order to describe, for instance, the magnetostriction measurements of Hendy *et al.* (1979) and Ott (1975). In addition to introducing a non-zero value of B_{α_2} for the hexagonal ions, of the magnitude used to obtain agreement with experiment in Fig. 7.13, it is probably also necessary to include B_{α_1} . Moreover, the magnetoelastic parameters for the cubic ions are presumably of the same order of magnitude as those on the hexagonal ions. This probably also applies to $B_2^0(c)$, neglected in eqn (7.4.6). The separation of the contributions from the hexagonal and the cubic ions to the c -axis bulk susceptibility as a function of temperature, accomplished through neutron-diffraction experiments by Rainford *et al.* (1981), indicates that not only is $B_2^0(c)$ non-zero, but the exchange between the c -axis components of the moments is also different from the corresponding coupling between the basal-plane components. The development of a MF model for Pr which describes its properties more accurately at elevated temperatures would benefit greatly from a more detailed examination of the excitations on the cubic sites, i.e. a determination of the energies of the excitations polarized in the c -direction, and the field-induced changes of these excitations, and of those polarized in the basal-plane and shown in Fig. 7.2.

The missing ingredients in the model presented here to describe Pr have a negligible influence on the pressure-induced ordered structure, and most of the observations made in this phase were explained by Jensen *et al.* (1987) utilizing only the information obtained from the zero-pressure studies of Houmann *et al.* (1979). Because the ordered moments in the antiferromagnetic phase are parallel to \mathbf{Q} , the change of the ground state affects primarily the longitudinal excitations, and the low-energy optical branch close to the ordering wave-vector is particularly strongly modified. Fig. 7.15 shows the experimental excitation energies of the optical modes in the ΓM -direction at 5.5 K, in the presence of a uniaxial pressure of 1.28 kbar, compared with the predictions of the RPA theory.

Under the conditions of the measurements, the analysis shows that the induced moments

$$\langle J_{i\eta} \rangle = \langle J_{\eta}(\mathbf{Q}) \rangle \cos(\mathbf{Q} \cdot \mathbf{R}_i + \varphi) \quad (7.4.7a)$$

are so small that the effective ($J = 1$)-model is adequate to describe the excitations, and the value of the third harmonic of the longitudinally ordered moments is only a few per cent of $\langle J_{\eta}(\mathbf{Q}) \rangle$. A full account of the structure would require specifying two phase constants, one for

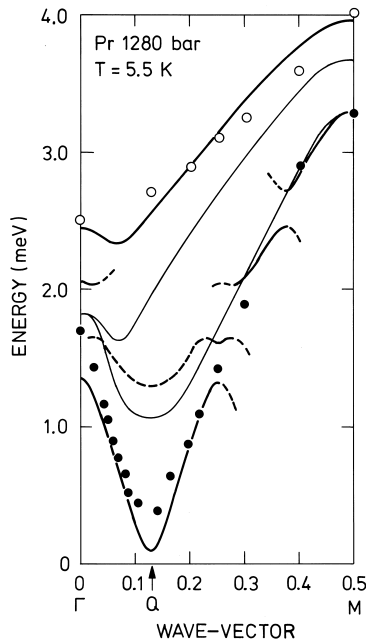


Fig. 7.15. The dispersion relations for the optical excitations in the antiferromagnetic phase of Pr at 5.5 K under an applied uniaxial pressure of 1.28 kbar. The ΓM direction shown is perpendicular to the pressure axis. The circles depict the experimental results obtained from inelastic neutron scattering, with solid and open symbols indicating the longitudinal and transverse branches respectively. The solid lines are the calculated RPA energies for the excitations, whereas the dashed lines indicate longitudinal modes of weaker intensity. The thin lines are the experimental dispersion relations in unstressed Pr, as in Fig. 7.1

each of the two sublattices. The difference between the two phases is approximately π , or approximately 0 if \mathbf{Q} , within the primitive zone, is replaced by $\mathbf{Q} + \mathbf{b}_3$. Introducing the relative magnetization σ by

$$\langle J_\eta(\mathbf{Q}) \rangle = M_\eta \sigma, \quad (7.4.7b)$$

where the matrix element is slightly dependent on the pressure ($M_\eta = 1.026\sqrt{10}$ at 1 kbar), we find that $\sigma \simeq 0.44$ under the conditions of Fig. 7.15. Because σ is still small, it may be utilized as an expansion parameter, both in the calculation of the ordered moments and also in the equations of motion determining the excitation spectrum. The ordering wave-vector is close to $\frac{1}{8}\mathbf{b}_2$, but whether the system is commensurate or not is not easy to decide from the experiments. In any case, this is not important for calculating the excitation spectrum, because distinctive effects of commensurability only appear in the order $\sigma^8 \approx 0.001$. The modulation of the length of the moments implies that the single-ion MF susceptibility is site-dependent, and the $\eta\eta$ -component is found to be

$$\chi_{\eta\eta}^o(j, \omega) = \frac{2n_{01}(j)M_\alpha^2\Delta \cos 2\theta_j}{(\Delta/\cos 2\theta_j)^2 - (\hbar\omega)^2} + \beta p_{01}(j)M_\alpha^2 \sin^2 2\theta_j \delta_{\omega 0}, \quad (7.4.8a)$$

equivalent to eqn (7.1.9) with $\langle J_{j\eta} \rangle = M_\eta n_{01}(j) \sin(2\theta_j)$, and $p_{01}(j)$ defined by

$$p_{01}(j) = n_0(j) + n_1(j) - n_{01}^2(j). \quad (7.4.8b)$$

$\Delta = \Delta_\eta(t_{11})$ is here the crystal-field splitting between the ground state $|0\rangle$ and the excited state $|1\rangle$ ($\equiv |1_a\rangle$ at zero stress) at the particular stress considered. In the incommensurate case, the coupling matrix determining the longitudinal component of the susceptibility tensor is of infinite extent. The situation is very similar to that considered in Section 6.1.2 and, as there, the coupling matrix may be solved formally in terms of infinite continued fractions. The only difference is that, in the present case, the single-site susceptibility is unchanged if the moments are reversed, which means that the coupling matrix only involves terms with n even (where n is the number of the Fourier component, as in (6.1.28)). Since the effective modulation wave-vector seen by the longitudinal excitations is $2\mathbf{Q}$ and not \mathbf{Q} , the acoustic and the optical modes propagating parallel to \mathbf{Q} may be treated separately, as the \mathbf{q} -dependent phase factor determining the effective coupling parameters $\mathcal{J}_{11}(\mathbf{q}) \pm |\mathcal{J}_{12}(\mathbf{q})|$, derived from the interactions in the two sublattices (see Section 5.1), is not affected.

To leading order, the modulation of the moments introduces a coupling between the excitations at wave-vectors \mathbf{q} and $\mathbf{q} \pm 2\mathbf{Q}$, and energy gaps appear on planes perpendicular to \mathbf{Q} passing through $n\mathbf{Q}$. When

$\mathbf{q} = \mathbf{Q}$, the coupling between the modes at \mathbf{Q} and $-\mathbf{Q}$ leads to an *amplitude mode* and a *phason mode*, corresponding respectively to an in-phase and a 90° out-of-phase modulation of the lengths of the moments. The energies of the two longitudinal modes at $\mathbf{q} = \mathbf{Q}$ are approximately given by

$$\begin{aligned} E_{\text{amplitude}} &\simeq \frac{\sqrt{3}}{2} \sigma \Delta \\ E_{\text{phason}} &\simeq \left(\frac{1}{8} \beta \Delta \bar{p}_{01} \right)^{1/2} \sigma \Delta, \end{aligned} \quad (7.4.9)$$

where \bar{p}_{01} is the average value of $p_{01}(j)$. The scattering intensity, proportional to $1/[\hbar\omega\{1 - \exp(-\beta\hbar\omega)\}]$, of the lowest-lying phason mode is much larger than that of the amplitude mode. The low-intensity amplitude mode is indicated by the dashed line at \mathbf{q} -vectors close to \mathbf{Q} in Fig. 7.15, and it was not clearly resolved in the experiments. The phason mode has a dispersion relation, indicated by the solid lines in the figure, which increases linearly from the magnetic Bragg peak at \mathbf{Q} , except for the presence of the small gap E_{phason} at $\mathbf{q} = \mathbf{Q}$. In the incommensurate case, the free energy is invariant to a change of the phase constant φ in (7.4.7), so that the longitudinal component of the zero-frequency susceptibility diverges at the wave-vector \mathbf{Q} . The corresponding generator of an infinitesimal phase shift is $1 - i\delta\varphi \sum_j (|1 \rangle \langle 1|)_j$. If this generator commuted with the Hamiltonian, a specific choice of φ would break a continuous symmetry of the system, implying the presence of a well-defined linearly-dispersive Goldstone mode, as discussed in Section 6.1. However, as may be verified straightforwardly, it does not in fact commute with the Hamiltonian. On the contrary, within the RPA the longitudinal response contains an elastic contribution, due to the final term in (7.4.8a), and hence the scattering function contains a diffusive peak at zero frequency. It is the intensity of this peak which is found to diverge in the limit $\mathbf{q} \rightarrow \mathbf{Q}$. As \mathbf{q} departs from \mathbf{Q} , the diffusive response at zero frequency rapidly weakens, and the phason mode begins to resemble a Goldstone mode. The presence of the inelastic phason mode at the wave-vector \mathbf{Q} can be explained as a consequence of the modulation of the population difference $n_{01}(j)$, which is proportional to \bar{p}_{01} . This mode corresponds to an oscillation of the phase-constant φ in (7.4.7), except that the adiabatic condition, which applies within the RPA as soon as the oscillation frequency is non-zero, constrains $n_{01}(j)$ to remain constant, without participating in the oscillations. This condition, in turn, gives rise to the restoring force which determines the frequency of the oscillations. However, if the oscillations are so slow (i.e. essentially zero in the present approximation) that $n_{01}(j)$ can maintain its thermal-equilibrium value, there are no restoring forces. In the zero-temperature limit, \bar{n}_1 vanishes exponentially, in which case $n_{01}(j) = 1$, and the diffusive elastic response disappears together with E_{phason} . The

gap also vanishes in the other limit when $\sigma \rightarrow 0$, as does the amplitude-mode energy gap, reflecting the soft-mode nature of the transition in this approximation. In the above discussion, we have assumed that the system is incommensurate. In a commensurate structure, the free energy is no longer invariant to an overall phase shift of the structure, and the longitudinal susceptibility does not diverge at \mathbf{Q} . Because of the small value of σ^8 , however, it is close to divergence. The phason-mode energy gap stays non-zero at $T = 0$ in the commensurate case, but it is estimated to be only about 0.03 meV at 1 kbar.

Even at the lowest temperatures reached in the inelastic neutron-scattering experiments, quite strong line-broadening of the low-lying longitudinal excitations was observed in the ordered phase. There are several mechanisms which may lead to non-zero linewidths. One possibility, if the ordering is incommensurate, is a broadening of the excitation peaks analogous to that illustrated in Fig. 6.3 in Section 6.1.2. However, the off-diagonal coupling terms, corresponding to γ_n in (6.1.30), are here multiplied by σ^2 , which means that the continued-fraction solution, although infinite, converges very rapidly without producing linewidth effects of any importance. The $1/Z$ -expansion, discussed in Section 7.2, accounts very well in first order in $1/Z$ for the lifetime effects observed in paramagnetic Pr, as shown in Fig. 7.4. In this order, the intrinsic-linewidth effects vanish exponentially at low temperature, and they should be negligible in the temperature range of the ordered phase, with the important exception that the elastic RPA response acquires a non-zero width. To first order in $1/Z$, δ_{ω_0} in eqn (7.4.8a) is replaced by a Lorentzian $i\Gamma/(\hbar\omega + i\Gamma)$, with $1/\Gamma \simeq \bar{n}_{01}^2(\pi/2)\mathcal{N}_\eta(\Delta)$, where $\mathcal{N}_\eta(E)$ is the density of states of the η -polarized part of the excitation spectrum. Due to the large value of Γ , estimated to be about 1 meV, the RPA predictions for the behaviour of the phason modes near the ordering wave-vector are strongly modified. Instead of an elastic diffusive and an inelastic, adiabatic phason mode, the theory to this order predicts only one mode at zero energy, but with non-zero width, when \mathbf{q} is close to \mathbf{Q} . An inelastic low-energy peak develops only at a distance of about $0.03|\mathbf{b}_1|$ from \mathbf{Q} . The exchange-enhancement factor in the scattering function causes the width of the Lorentzian near \mathbf{Q} to be much less than 2Γ . Formally the width tends to zero when $\mathbf{q} \rightarrow \mathbf{Q}$, but it is more precisely the intensity which diverges, while strong inelastic tails remain at $\mathbf{q} = \mathbf{Q}$, in accordance with the experimental results.

As was mentioned in Section 7.2, the $1/Z$ -expansion of the effective medium theory was extended to second order in $1/Z$ by Jensen *et al.* (1987). The second-order modifications are important here, but not in the zero-stress case considered in Fig. 7.4, because the low-temperature energy gap of about 1 meV in the excitation spectrum is suppressed by

the uniaxial pressure. The gapless excitation-spectrum in the ordered phase implies that the linewidth effects are predicted to vary smoothly with temperature, and to stay non-zero at $T = 0$, when the second-order contributions are included. We note that the imaginary part of the self-energy is now non-zero below the RPA-excitonic band in the paramagnetic phase, and that it generates an appreciable low-energy scattering at the ordering wave-vector, just above T_N , changing the inelastic critical excitation into a diffusive mode of diverging intensity. Hence a true 'soft-mode transition', as found in the zeroth or first order of $1/Z$, is no longer predicted, but the low-energy effect is far too weak to account for the observed behaviour of the neutron-diffraction satellite. The inclusion of the second-order effects in the theory clearly improves the agreement with the experimental results. However, even though the $1/Z^2$ -theory predicts a non-zero linewidth in the limit $T \rightarrow 0$, the effect is so small, at energies below 1 meV, that it can be neglected in comparison with the contribution due to the scattering against electron-hole pair excitations of the conduction electrons, discussed in Section 7.3.2. The importance of this mechanism has been estimated reasonably accurately, and it leads to a linewidth of the order of 0.15 meV for the optical modes close to \mathbf{Q} . When all contributions are included, the theory indicates that the amplitude mode should have been observable at $\mathbf{q} = \mathbf{Q}$ at the lowest temperatures, in contrast to the experimental results, but otherwise its predictions are found to agree well with the main features of the observations.